

[Click here to view linked References](#)Manuscript submitted to **Biophysical Journal****Article**

Magainin 2 and PGLa in Bacterial Membrane Mimics III: Membrane Fusion and Disruption

Ivo Kabelka^{1,2,†}, Vasil Georgiev^{3,†}, Lisa Marx^{4,5}, Peter Pajtinka^{1,2,6}, Karl Lohner^{4,5}, Georg Pabst^{4,5}, Rumiana Dimova³, and Robert Vácha^{1,2,6,*}¹CEITEC – Central European Institute of Technology, Masaryk University, Kamenice 5, 625 00 Brno, Czech Republic²National Centre for Biomolecular Research, Faculty of Science, Masaryk University, Kamenice 5, 625 00 Brno, Czech Republic³Max Planck Institute of Colloids and Interfaces, Science Park Golm, 14424 Potsdam, Germany⁴University of Graz, Institute of Molecular Biosciences, Biophysics Division, NAWI Graz, Graz, Austria⁵BioTechMed Graz, Austria⁶Department of Condensed Matter Physics, Faculty of Science, Masaryk University, Kotlářská 2, 611 37 Brno, Czech Republic

*Correspondence: robert.vacha@mail.muni.cz

†These authors contributed equally.

ABSTRACT We previously speculated that the synergistically enhanced antimicrobial activity of Magainin 2 and PGLa is related to membrane adhesion, fusion, and further membrane remodelling. Here, we combined computer simulations with time-resolved *in vitro* fluorescence microscopy, cryogenic electron microscopy (cryo-EM), and small-angle X-ray scattering (SAXS) to interrogate such morphological and topological changes of vesicles at nanoscopic and microscopic length scales in real time. Coarse-grained simulations revealed the formation of an elongated and bent fusion zone between vesicles in the presence of equimolar peptide mixtures. Vesicle adhesion and fusion was observed to occur within few seconds by cryo-EM and corroborated by SAXS measurements. The latter experiments further indicated continued and time-extended structural remodelling also for individual peptides or chemically-linked peptide heterodimers, but with different kinetics. Fluorescence microscopy further captured peptide-dependent adhesion, fusion, and occasional bursting of giant unilamellar vesicles already few seconds after peptide addition. The synergistic interactions between the peptides shorten the time response of vesicles and enhance membrane fusogenic and disrupting properties of the equimolar mixture compared to the individual peptides.

STATEMENT OF SIGNIFICANCE

MG2a and L18W-PGLa are prominent antimicrobial peptides with an enigmatic mechanism of synergism. Here, we capture the time evolution of membrane remodelling that arise from the interactions between the peptide equimolar mixture and lipid vesicles, which mimic cytoplasmic membranes of Gram-negative bacteria. Using a variety of techniques, we demonstrate that mutual interactions between both peptides enhance the kinetics and extent of membrane disruption and fusion.

INTRODUCTION

Magainin 2 and PGLa, or alternatively amidated magainin 2 (MG2a) and L18W-PGLa, are well-studied pairs of antimicrobial peptides derived from the African clawed frog with synergistic activity against Gram-negative bacteria (1, 2) and various lipid-only mimics of bacterial cytoplasmic membranes (3–9). Due to significant discrepancies between individual reports, however, the exact mechanism of synergism remains inconclusive. For example, synergistically increased leakage of fluorescent dyes from vesicles was interpreted

as resulting from toroidal pore formation, where peptides orient roughly perpendicular to the membrane plane (1). In contrast, solid state NMR experiments reported peptide orientation parallel to the membrane plane for the same membrane composition (3, 5). We showed recently that the peptides' synergistic behaviour depends strongly on the investigated lipid mixture (2), implying that only experiments with the same membrane composition should be compared. In particular, we demonstrated that the membrane needs to have a net negative surface charge and store a net negative intrinsic curvature stress to exhibit a synergism that correlates with the peptides' bacterial activity. As a result, palmitoyl oleoyl phosphatidylethanolamine (POPE): palmitoyl oleoyl phosphatidylglycerol (POPG) (3:1 mol:mol) mixture emerged as reasonable first order proxy of the cytoplasmic membrane of Gram-negative bacteria (2).

In the previous parts of this paper series, (7, 8), we showed that the equimolar mixture of MG2a and L18W-PGLa peptides causes adhesion between POPE:POPG (3:1 mol:mol) bilayers, leading to the transformation of large unilamellar vesicles (LUVs) into multibilayers with a collapsed interstitial water layers and occasional fusion stalks. Moreover, we found

that the two peptides self-assemble on the membrane forming dimers (mostly surface-aligned parallel heterodimers) already at low concentrations, and then further aggregate into fibril-like structures between two membranes. Finally, we observed the formation of a sponge phase, resembling a molten cubic phases as a salient feature of the peptides' synergistic activity. The dynamics of described events, however, remained unexplored.

In this work, we examined the time evolution of the systems to interrogate the formation of collapsed multibilayers and the sponge phase. Further, adhesion, fusion or rupture of the POPE:POPG bilayers may occur at very different time-points for the individual peptides or the peptide mixture, and provide important clues to the role of peptide/peptide and peptide/lipid interactions. We therefore combined computer simulations of whole vesicles with time-lapse fluorescence microscopy, time-resolved small-angle X-ray scattering (SAXS) and cryogenic electron microscopy (cryo-EM). This variety of techniques allowed us to explore the membrane behaviour with various temporal resolution and in a wide range of length scales from tens of nanometers to tens of micrometers.

MATERIALS AND METHODS

MD Simulations

Molecular dynamics (MD) simulations were performed using GROMACS version 2016.2 (10, 11). Coarse-grained MARTINI 2.2 force field (12–14) was employed with the simulation time step set to 20 fs. Constant temperature of 310 K was maintained via velocity-rescaling thermostat (modified with a stochastic term) (15) with a coupling constant of 1.0 ps. For proper temperature distribution, two separate baths were coupled to protein-lipid and solvent beads. The pressure was kept at 1 bar using the Parrinello-Rahman barostat (16, 17) with a semi-isotropic coupling scheme and a coupling constant of 12 ps. All non-bonded interactions, including van der Waals forces were cut-off at 1.1 nm. The relative dielectric constant was set to 15.

Due to the coarse-graining and resulting inability of MARTINI force field to fold proteins, fully α -helical secondary structure was imposed on the peptides throughout the entire simulation run. The peptide C-terminal capping was modeled by the removal of the backbone bead charge and changing the bead type to neutral.

Fusion of lipid vesicles

A lipid vesicle was prepared using CHARMM-GUI web server (18). Mixture of 3000 POPE:POPG (3:1 mol:mol) lipid molecules was used to prepare a lipid vesicle with diameter of ~21 nm. Subsequently, the system was solvated with ~60 water beads (one bead represents four water molecules) per lipid. For equilibration of the pressure inside and outside the vesicles, several membrane pores were created and maintained by an inverted cylindrical flat-bottomed potential with a force

constant of $1000 \text{ kJ mol}^{-1} \text{ nm}^{-2}$. Starting from 2 nm, the pore was gradually closed over the course of the ~140 ns long equilibration.

After equilibration, the vesicle (without any pores) was also used to prepare systems with peptides at $[P]/[L]$ ratio of 1/42 or 1/21. MG2a and L18W-PGLa peptides were added (in equimolar concentration) on the outer surface of the vesicle with random initial positions and orientations.

In all systems, Na^+ and Cl^- ions were added at concentration of 130 mM in the whole system with excess ions to neutralize the system net charge. After energy minimization, all systems were equilibrated further for 1 μs . Finally, the vesicles were used to create several systems with one or two vesicles.

In the first simulated scenario, a single vesicle was interacting with itself over the periodic boundary conditions. In such a system, full vesicle fusion leads to the formation of a periodic lipid tube. Systems with two peptide to lipid ratios, $[P]/[L] = 1/42$ and $1/21$, were considered and the total simulation length was 40 μs .

In the second simulation scenario, the single vesicle system was duplicated, translated, and merged to create a system with two vesicles. For computational efficiency, the vesicles were limited in lateral diffusion and kept in the box center within a cylindrical volume. A cylindrical flat-bottomed potential was applied on all lipid beads that moved further than 14 nm from the cylinder center. The following systems were explored: 1) vesicles without peptides, 2) with peptides on a single vesicle at $[P]/[L] = 1/21$, 3) vesicles with peptides on both vesicles at $[P]/[L] = 1/42$, and 4) vesicles with peptides on both vesicles at $[P]/[L] = 1/21$. The total simulation length of each simulation was 100 μs for the system without peptides and 150 μs for systems with peptides. All simulation input files can be found in Simulations.zip in the Supplementary Information.

Materials

The lipids 1-palmitoyl-2-oleoyl-sn-glycero-3-phospho-(1'-rac-glycerol) sodium salt (POPG), 1-palmitoyl-2-oleoyl-sn-glycero-3-phosphoethanolamine (POPE) and the fluorescent probe 1,2-dioleoyl-sn-glycero-3-phosphoethanolamine-N-(lissamine rhodamine B sulfonyl) (DPPE-Rh) were obtained from Avanti Polar Lipids (Alabaster, AL). HEPES and NaCl were purchased from Carl Roth (Karlsruhe, Germany). Bovine serum albumin (BSA) was obtained from Sigma-Aldrich (St. Louis MO), polyvinyl alcohol (PVA, with MW 145000) – from Merck (Darmstadt, Germany), and fluorescein – from Thermo Fisher Scientific (Waltham, MA). L18W-PGLa, MG2a and the chemically linked (at peptides' C-termini) heterodimer L18W-PGLa:MG2a, denoted in the following as hybrid peptide, were obtained in lyophilized form (purity >95%) from PolyPeptide Laboratories (San Diego, CA). All other chemicals were obtained from Sigma-Aldrich in pro analysis quality.

Vesicle preparation

Large unilamellar vesicles (LUVs): Lipid stock solutions for sample preparation were prepared in organic solvent chloroform/methanol (9:1, vol/vol) and phosphate assayed for quantification of lipid content (19). Thin lipid films were prepared by mixing appropriate amounts of lipid stock solutions, followed by solvent evaporation under a nitrogen stream at 35°C and overnight storage in a vacuum chamber. The dry lipid films were rehydrated using HEPES-buffered saline (HBS) (10 mM HEPES, 140 mM NaCl, pH 7.4) and equilibrated for one hour at 40°C followed by 5 freeze-and-thaw cycles using liquid N₂ and intermittent vortex mixing. LUVs were obtained by 31 extrusions with a hand held mini extruder (Avanti Polar Lipids, Alabaster, AL) using a 100 nm pore diameter polycarbonate filter and phosphate assayed afterwards to determine the resulting lipid concentration.

For Cryo-EM, the protocol for LUV preparation was slightly modified, because the purchased lipids were already dissolved in chloroform. Dry lipid films were hydrated for 20 minutes with intermittent mixing. Subsequently, 15 freeze-and-thaw cycles and 50 cycles of extrusion were performed with polycarbonate filter having either 50 nm or 100 nm pores.

Giant unilamellar vesicles (GUVs): A 4 mM lipid stock solution in chloroform containing POPE, POPG (in molar ratio 3:1) and 0.1 mol% of the fluorescent probe (DPPE-Rh) was prepared and stored at -20°C. GUVs were formed using the gel-assisted method (20). Briefly, HBS containing 5% PVA was prepared. The PVA was dissolved under stirring for 1 hour at 90°C. 50 μ L of the PVA solution were spread on a glass slide and dried for 1 h at 60°C. 5 μ L of the lipid stock solution were deposited on the PVA-coated glass. The glass was then kept for 1 h under vacuum at room temperature to evaporate the chloroform and afterwards assembled into a chamber with a 2 mm-thick Teflon spacer. The chamber was filled with HBS containing 10 μ M fluorescein. To ensure that the PVA film does not influence peptide-membrane interactions, we harvested the vesicles after 5–10 min from the formation chamber for experiments. Only fresh vesicle solutions were used in this work.

SAXS

SAXS data were collected at the highflux Austrian beamline at Elettra Synchrotron in Trieste, Italy (21) and SAXS patterns were recorded using a Pilatus 1 M detector (Dectris, Baden-Daettwil, Switzerland) at a photon energy of 8 keV and a wavelength of 0.155 nm, spanning the q -range from 0.1 nm⁻¹ to 5 nm⁻¹, and further processed with FIT2D (22).

Lipids and peptides were mixed using an automatic sample changer and automatically injected into a custom-build cell, allowing for precise measurements of very small volumes (10 μ L), immediately after mixing (see, e.g. (23)). Measurements were performed at a lipid concentration of 20 mg/ml at 37°C. Peptide kinetics were measured starting 30 s after lipid-peptide mixing with an acquisition time of 1 s per frame and a hold

time of 10 s between the individual exposures.

For end-state measurements, lipids were mixed with peptides and incubated at 37°C for at least 7 h. The samples were measured using 12 frames of 10 s exposure each and a hold time of 12 s between each measurement. Data were analyzed based solely on Bragg peak positions fitting the data with a Lorentzian function. According to Bragg's law, the reported d -spacing values are given by $d = 2\pi/q_h$, where q_h is the peak position. Further, the average number of lamellae per scattering domain was estimated using $l = 2\pi/(d \omega_1)$, where ω_1 is the full width at half maximum of the first order lamellar peak.

Cryo-EM Experiments

For 30 s, 2 μ L of LUVs were equilibrated on a freshly glow discharged TEM grids (Quantifoil, Cu, 200 mesh, R2/1) in the climate chamber of the ThermoScientific Vitrobot IV (25°C, 95% rel. humidity). Subsequently, the LUVs were incubated with either 2 μ L of buffer (control specimen) or L18W-PGLa:MG2a 1:1 (mol:mol) peptide solution ([P]/[L] ratio of 1/50) for 0, 20, and 60 seconds, blotted against filter paper, and vitrified into liquid ethane. The samples were subsequently loaded into ThermoScientific Talos Arctica transmission electron microscope operating at 200 kV. The images were collected on ThermoScientific Falcon 3EC direct electron detection camera operating in charge integration mode using SerialEM software. The overall dose per single image did not exceed 20 e/A².

Fluorescence microscopy and microfluidics of GUVs

GUVs were observed with a 40 \times air objective on a Leica TCS SP5 confocal microscope (Mannheim, Germany) with the heating stage set to 27°C. DPPE-Rh was excited with a diode-pumped solid-state laser at 561 nm and the fluorescence signal was collected in the range 570–635 nm. Fluorescein was excited with the 488 nm line of an Argon laser and the signal was collected between 495–555 nm. Sequential scanning was performed to avoid crosstalk between the fluorescence signals. The bulk measurements for the vesicle survival as a function of peptide concentration were conducted on a Axio Observer D1 microscope (Zeiss, Germany) using a 20 \times air objective. The vesicles were incubated for 10 minutes with the desired concentration of either 1:1 L18W-PGLa:MG2a mixture or the hybrid peptide. Then a 10 μ L drop was placed in the observation chamber and the vesicles were let to settle for 5 min. The whole area with the settled GUVs was scanned and the vesicles were counted. The total lipid concentration, 10 μ M, and related [P]/[L] ratio in these experiments was calculated from the amount of lipids used to prepare the vesicles and taking in account the subsequent dilution steps.

The total lipid concentration, 10 μ M, and related [P]/[L] ratio in these experiments was calculated from the amount of

lipids used to prepare the vesicles and taking into account the subsequent dilution steps.

To exchange the solution around the vesicles, we introduced the GUVs in a microfluidic device (24). The microfluidic chips were provided by courtesy of T. Robinson. The external medium (HBS, 10 μ M fluorescein) was replaced with a solution of the peptides dissolved in HBS. The device allows trapping of GUVs by microfluidic posts, exchanging the outer solution and observing the same vesicle before and after the peptide has reached the membrane. This single-vesicle approach allows to exclude possible artefacts associated with vesicle preparation (for example, avoiding work with leaky or damaged vesicles). The microfluidic chips were first coated with 2% BSA dissolved in HBS. Then, 50 μ l of the obtained GUVs suspension were loaded into the microfluidic device at a flow rate of 2 μ L/min. To control the flow, the chip was connected to a syringe pump (neMESYS, CETONI, Korbussen, Germany). Afterwards, a fluorescein-free solution containing 100 μ M of the desired peptide (L18W-PGLa, MG2a, a 1:1 mixture of both, or the hybrid peptide) was introduced in the microfluidic chamber with a flow rate of 0.5 μ L/min. The external osmolarity of the vesicles was adjusted (with glucose) to match that of the internal solution using an osmometer (Osmomat 030, Gonotec, Germany).

RESULTS

In order to visualise the synergism of L18W-PGLa and MG2a peptides in POPE:POPG bacterial membrane mimics in a wide range of time and length scales, we combined MD simulations and time resolved experiments (cryo-EM, SAXS, and fluorescence microscopy). MD simulations provide nearly atomistic resolution of small interacting vesicles at timescales below 1 ms. In cryo-EM, we interrogate changes of large unilamellar vesicles at nanometer scale just few seconds after the peptide addition. SAXS experiments were used to complement the two methods with time scale up to several hours. Finally, fluorescence microscopy directly visualise the peptide induced modifications of giant unilamellar vesicles with resolution below seconds. All experiments were performed above the gel-fluid phase coexistence regime of POPE/POPG mixtures (25).

MD simulations

In our previous simulations, we have observed heterodimers of MG2a and L18W-PGLa to induce a formation of fusion stalk between two planar membranes (8). However, such an observation could be affected by the topology of the simulation box containing two planar bilayers. Therefore, we performed simulations of POPE:POPG (3:1 mol:mol) lipid-vesicle(s) both without and with peptides adsorbed on the outer surface. The equimolar mixture of peptides was added at $[P]/[L] \sim 1/42$ and $1/21$, consistent with the first and second paper of this series (7, 8).

Figure 1: Progression of vesicle fusion with peptides (equimolar mixture of L18W-PGLa:MG2a) at $[P]/[L] = 1/42$. Slices (denoted by the dashed lines in the second row of snapshots) through the fusion stalk are shown in the bottom row with the last three snapshots. Solvent and lipid head groups are not shown for clarity. Lipid tails: gray sticks; POPE and POPG phosphates: orange and yellow spheres, respectively. Peptide residues nonpolar: gray; polar: green; acidic: red; basic: blue.

Firstly, we studied systems with a single vesicle interacting with itself over the periodic boundary conditions. Fig. 1 shows representative snapshots and Fig. 2 schematic illustrations for $[P]/[L] = 1/42$. After the initial approach of the vesicle hemispheres, the bilayers adhered together via peptides (regardless of their oligomerisation state or identity). Subsequently, fusion was nucleated by one heterodimer in the contact zone between the bilayers. The formation of a fusion stalk was initiated by a reorientation and insertion of one of the lipid's tails between peptides in a heterodimer the same way as described in our previous paper (8). A quick reorientation of neighbouring lipids resulted in formation of a fusion stalk between the outer leaflets of vesicle hemispheres. The stalk grew, forming a contact zone structure with a bicelle-like cross section in the lateral cut connecting the two hemispheres. Each 'cap' of the bicelle-like contact zone contained one peptide from the fusion-initiating heterodimer. As the contact zone extended along the long axis of the 'bicelle', it started to bend and form a horseshoe-like structure with only a small opening after 1 μ s. Except for the end caps, no peptides resided in the contact zone. In the simulation, it took about $\sim 20 \mu$ s before the opening fully closed, trapping a L18W-PGLa peptide inside a new vesicle-like structure. On the 40 μ s simulation time scale, the fusion did not progress further. In the system with higher peptide concentration ($[P]/[L] = 1/21$), we observed only the adhesion of the two vesicle hemispheres, see Fig. S1. During this simulation, an increasing number of peptides was recruited to the contact area, slightly flattening the vesicle hemispheres. The lack of fusion stalk formation in this system demonstrates a stochastic nature of the stalk formation.

Secondly, we simulated systems with two interacting vesicles. In the system without peptides, we observed the vesicles to repeatedly get into contact and separate again, see Fig. S2. For vesicles with peptides at $[P]/[L] = 1/42$, we saw only the adhesion of the two vesicles on the simulated time scale of 150 μ s, see Fig. S3. The first contact between the two vesicles was mediated by a single peptide, however, this interaction was not sufficient and the vesicles separated. During the second contact, a peptide dimer present on one vesicle anchored to the other vesicle. Subsequently, more peptides were recruited to this interaction site and the vesicles adhered to each other. In the same simulation system, but at $[P]/[L] = 1/21$, the vesicles adhered to each other after the first contact within 1 μ s. The fusion stalk, having a similar

Figure 2: Schematic illustration of vesicle fusion. A) Vesicle approach, B) single lipid (highlighted in red) connecting both vesicles, C) fusion of the outer membrane leaflets, D) formation of a small vesicle-like structure between the large vesicles, E) progression of the fusion stalk formation shown as an xy-cross section. The green-shaded area shows regions where peptides were residing during simulation; individual peptides are not shown. For corresponding simulation snapshots see Fig. 1. (A–D) Side view of the vesicles and (E) slice through the fusion stalk are shown.

structure as the one in Fig. 2, appeared after 3 μ s and slightly-curved and widened within ~ 6 μ s. In the initial stages of fusion, the peptides were located only at the ends of the fusion neck (as indicated in Fig. 2E). The second contact site between the vesicles changed the mutual orientation of the vesicles and offset the fusion neck from the center to the side, see ~ 7 μ s in Fig. S4. The fusion neck bulged outwards, which enabled the peptides to diffuse on this positively curved surface, see Fig. S5 and movie S1.

We also prepared a system with peptides adsorbed on only one of the two vesicles ($[P]/[L] = 1/21$), to see whether peptides adsorbed to both vesicles are necessary to initiate vesicle adhesion and fusion, see Fig. S6. Indeed, we found that adhesion of vesicles and subsequent fusion proceeded as in the above-described systems with a single vesicle and $[P]/[L] = 1/42$. It is worth noting that the peptides did not reside on the fusion neck apart from the two peptides at the ends of the fusion-neck as before, see Fig. S6 at 6.2 μ s. After closing of the neck, all peptides were adsorbed almost exclusively on the spherical surfaces of large vesicles and avoided the fusion neck, see movie S2. The concentration of peptides on both fusing vesicles was uneven at the end of the simulation due to the limited simulation length and the unfavorable diffusion through the fusion neck with a negative Gaussian curvature.

Cryo-EM

We performed cryo-EM experiments to verify the peptide-induced vesicle adhesion and fusion. We prepared two samples of POPE:POPG (3:1 mol:mol) LUVs with diameters of 100 nm or 50 nm. The samples were vitrified at selected intervals (0, 20, and 60s) after the addition of peptides ($[P]/[L] = 1/50$; L18W-PGLa:MG2a equimolar mixture).

The reference system with 100 nm sized vesicles without peptides contained mostly unilamellar vesicles (Fig. 3 A). The majority of the vesicles was located on the grid or close to the edges. It is possible that a considerable amount of vesicles was removed during blotting. Interestingly, we observed the immediate (within ~ 5 s) formation of vesicle adhesion seen as frequent close contacts between two lipid bilayers. 20 s after peptide addition, the fusion had progressed and the adhered vesicles were separated by what appears to be only a single lipid bilayer (Fig. 3 C, top). Additionally, we observed some multilamellar vesicles (Fig. 3C, bottom). Very large vesicles, hundreds of nanometers in size, were formed in samples vitrified 60 s after peptide addition (Fig. 3D). Sites

of possible ongoing fusion events are marked by red arrows. Additional images are shown in Fig. S7; see also CryoEM.zip in Supplementary information for large number of system views.

Time-resolved SAXS

We performed SAXS experiments to investigate the structural changes in the membrane induced by the peptides on supramolecular length scales. Vesicles composed of POPE:POPG 3:1 mol:mol without peptides (reference systems) showed a purely diffuse scattering pattern originating from positionally uncorrelated lipid bilayers (Fig. 4 A), as expected for LUVs. Upon the addition of peptide ($[P]/[L] = 1/25$) we observed in all cases a rapid, within 30 s, formation of a lamellar phase with a collapsed interbilayer spacing (Fig. 4 A, C and Fig. S8), as detailed previously (8). Also the reported sponge phase for the 1:1 peptide mixture (8), signified by a broad peak at $q \sim 0.08$, formed immediately. The previously described cubic phase, only found for the hybrid peptide, formed later and appeared only in the ‘end-state’ measured 7 h after peptide addition (Fig. 4A).

Interestingly, the sponge phase signature did not change significantly within the time scale of our experiments, while the sharp Bragg peaks corresponding to the lamellar phase showed pronounced kinetics. Addition of equimolar peptide mixtures or hybrid peptides led to a rapid precipitation of the sample, which reduced the amount of sample being hit by the X-ray beam. This explains the increased noise of scattering data at longer times. Focusing on the evolution of the first order Bragg peak, the corresponding d -values exhibited a non-monotonic behaviour over time (Fig. 4 D), showing first a decrease over 10–20 min, followed by a slow increase. During this equilibration process, the observed d -values always followed the order $d(\text{MG2a}) > d(\text{L18W-PGLa}) > d(\text{L18W-PGLa:MG2a}) > d(\text{hybrid})$. At the same time we found that the estimated number of layers, participating in the formation of the lamellar phase increased – the exception being the equimolar peptide mixture – and was the highest for the hybrid peptide, followed by L18W-PGLa and MG2a. The number of positionally correlated layers was initially highest for peptide mixture, but then did not change significantly till the end of the experiment.

Figure 3: Cryo-EM images of POPE:POPG (3:1 mol:mol) LUVs A) without peptides, B) quickly (~ 5 s) after peptide addition, C) 20 s after peptide addition, D) 60 s after peptide addition. Yellow arrows point to adhesion regions between two bilayers, blue arrows show three conjoined vesicles, green arrows show multilamellar vesicles, and red arrows show putative vesicle fusion sites in presence of L18W-PGLa:MG2a 1:1 mol:mol mixture ($[P]/[L] = 1/50$). Scale bars correspond to 100 nm.

Figure 4: Structural SAXS kinetics induced by A) the hybrid peptide as observed in the evolution of SAXS patterns of pure POPE:POPG LUVs and at a $[P]/[L] = 1/25$ with B) the corresponding surface plot showing changes in the first order lamellar peak. Panel C) and D), respectively, show the changes in d -spacing and number of lamellar layers in POPE:POPG membrane mimics over time induced by L18W-PGLa, MG2a, the mixture 1:1 and the hybrid at a $[P]/[L] = 1/25$.

Fluorescence microscopy and microfluidic manipulation of GUVs

GUVs are convenient model systems for real-time interrogation of the membrane response (26–28) and allow for direct microscopy visualization of the membrane morphology (29, 30). Here, we probed the vesicles' response to (i) the individual peptides MG2a or L18W-PGLa, (ii) an equimolar mixture of both peptides, and (iii) the hybrid peptide. The GUVs were studied above the gel-fluid transition temperature (25) and no domains were observed in the system, see movie S3. The GUVs were investigated either in bulk studies of mixing and subsequent microscopy observation, or in microfluidic chips allowing us to follow the behaviour of individual vesicles upon solution exchange. Fluorescein, which was encapsulated in the GUVs served as a marker for membrane leakage. That is, the decrease of fluorescence signal in the vesicles signifies peptide-induced membrane permeation, including the transient formation of pores, allowing the dye molecules to 'escape' from the vesicles interior. Flushing the fluorescein-free peptide solution into the microfluidic chip enhances the vesicle contrast as the free fluorescein outside the GUVs is washed away. Simultaneously, the decrease in the fluorescein signal of the vesicle surroundings gives information about the timing of peptide arrival at the inspected GUV.

The GUVs exhibited different behaviour depending on the peptide type ($[P] = 100 \mu\text{M}$). Introducing L18W-PGLa resulted in vesicle-vesicle adhesion (as exhibited by the formation of flat contact zones between neighbouring vesicles, see Fig. S9 A) and subsequent fusion (Fig. 5 A); note that vesicle adhesion was not observed when a peptide-free buffer was flushed (see Fig. S10). GUVs which fused with each other, preserved the fluorescence signal in their interior, which indicates lack of leakage (see movie S4). The vesicles preserved their contrast also in the presence of MG2a (see Fig. S11 and movie S5), however, vesicle bursting (instead of fusion) was observed (Fig. 5 B). In contrast, all vesicles ruptured after introducing the equimolar peptide mixture or the hybrid peptide (movie S6 and S7). In the case of the peptide mixture, around 67 % of the GUVs ($N = 32$) lost their contrast before bursting. The leakage with subsequent bursting can be seen in Fig. 5 C and movie S6. The video shows distinct signatures of GUV bursting with/without leakage with a time

lag of about 162 s after arrival of the peptides. In addition, GUV-GUV adhesion and fusion were also observed for the peptide mixture prior to GUV rupture. However, vesicle bursting was the dominating event. Before bursting, the GUV surface area decreased (Fig. S13), suggesting the potential formation of e.g., folds, buds, or tubes to release the peptide induced membrane stress. However, the nature of these structures remained below our optical resolution. After bursting, the lipid membrane rearranged into micron-size vesicle-like structures with boundaries which are optically thicker than those of single-bilayer vesicles (see Fig. 5 C or Fig. S12). The fluorescence signal in these structures was heterogeneous and corresponded to roughly 2 to 7 fold the fluorescence of a single bilayer. Occasionally, the aggregates were observed even prior to vesicles bursting, see the lower row of Fig. 5 C. In the presence of the hybrid peptide, the vesicles ruptured without leakage (Fig. 5 D). Also, no other events but bursting were observed for the hybrid peptide. We observed, however, a significant difference in GUV bursting rate when comparing hybrid peptide and equimolar peptide mixture at equal $[P]$ in solution. All GUVs ruptured already after 98 s in the presence of the hybrid peptide, while in the case of the 1:1 peptide mixture all vesicles were burst after ~ 4 minutes (Fig. 6 A).

Introducing the peptide solution in the microfluidic chip causes a gradual increase of the peptide concentration as the external solution around the vesicles is exchanged (in practice, the green curve in Fig. 5 E inversely reflects the peptide concentration changes). We observed the fraction of ruptured vesicles to increase during this process, suggesting concentration dependent activity. Thus, we screened a range of peptide concentrations to examine at which conditions vesicle bursting becomes pronounced. This experiment was performed in the bulk. That is, the GUVs were incubated for 5 minutes with the desired concentration of either the hybrid peptide or the 1:1 L18W-PGLa:MG2a mixture. In both cases, no vesicles survived for peptide concentrations larger than $10 \mu\text{M}$ (the lipid concentration was roughly estimated to be $10 \mu\text{M}$, $[P]/[L]=1/1$). However, the GUVs were destabilized by the hybrid peptide already at much lower concentration, compared to the response to the peptide mixture: 93% of the GUVs ruptured at $1.75 \mu\text{M}$ hybrid peptide, while no vesicle bursting was observed at the same concentration of the 1:1

Figure 5: Effect of L18W-PGLa, MG2a, their equimolar mixture and the hybrid peptide on GUVs (POPE:POPG = 3:1 mol:mol) labeled with DPPE-Rh (red) and encapsulating fluorescein (green). The vesicles were trapped in a microfluidic chamber (the black shadows in A represent the posts holding the vesicles in place). Time zero indicates the time of peptide arrival. A) Vesicle fusion in response to PGLa introduced at a concentration of 100 μ M. Because of the flow (applied from the right) and the resulting excess area, the fused vesicle deforms partially entering the space between the microfluidic posts (black). B) Interaction of MG2a (100 μ M) with the membrane results in vesicle bursting. C) Exposure to a mixture of both peptides, each at concentration of 50 μ M, causes vesicle bursting without and with poration. The arrows point to vesicles which porate and/or burst. In contrast, membrane leakage due to submicroscopic pores (as evidenced by slow decay of the fluorescence signal in the vesicle interior) was not detected in the presence of individual peptides. D) shows vesicle bursting in the presence of the hybrid peptide. The scale bars correspond to 25 μ m. E) Changes in the fluorescein signal in the external vesicle solution (green curve) and in the solution inside vesicles upon the application of L18W-PGLa:MG2a (1:1). Data for GUVs bursting with (blue curve) or without leakage (magenta curve); the arrowheads indicate the moment of bursting, which is followed by a decrease of the internal fluorescence until approaching background levels. Negative time corresponds to the time before the start of solution exchange followed by gradual peptide arrival (as monitored by the green curve; note that the apparent kink in the curve is due to axis scaling change).

Figure 6: Vesicles bursting caused by the 1:1 peptide mixture and the hybrid peptide ($[P] = 100 \mu$ M). (A) Bursting kinetics illustrated by the fraction of ruptured vesicles with time measured over populations of vesicles loaded in microfluidic chips. Time 0 indicates the peptide arrival in the vesicle trap. (B) Fraction of ruptured vesicles as a function of the peptide concentration. The measurements were performed in the bulk and on the average 3 samples were measured. The error bars correspond to standard deviation.

L18W-PGLa:MG2a mixture (Fig. 6 B).

DISCUSSION

We previously demonstrated that the synergistic behaviour of equimolar L18W-PGLa:MG2a mixtures is more complex than previously anticipated (2, 7, 8). In particular, ref. (8) suggested that these peptides could cause membrane adhesion and fusion in POPE:POPG (3:1 mol:mol) mimics of cytoplasmic membranes of Gram-negative bacteria. Here, we combined computer simulations with three different time-resolved experiments (cryo-EM, SAXS, and video microscopy) to directly capture such events in real time at microscopic to nanoscopic length scales in the same bacterial membrane mimics.

The applied experimental techniques consistently demonstrate that both AMPs alone are able to induce membrane adhesion, fusion, vesicle bursting, or the formation of MLVs with a collapsed interbilayer water spacing on the subminute to minute time scale. The higher propensity of MG2a to burst GUVs compared to L18W-PGLa (Fig. 5) might be related to increased peptide partitioning (9) (but see also paper IV of this series). Also differences in tension induced by insertion depth within POPE:POPG (both roughly parallel to the surface, but L18W-PGLa ‘sitting’ slightly deeper in the headgroup region than MG2a) (7) might contribute to the bursting induced by MG2a. The non-monotonous evolution of the lamellar

repeat distance of the collapsed multibilayers (Fig. 4) further suggests a rapid formation of MLVs (< 1 min) followed by an extended equilibration, which will involve diverse processes, such as peptide translocation, membrane fusion, etc.

For equimolar mixtures of L18W-PGLa:MG2a, these effects are significantly accentuated and occur on faster time scales (see in particular Fig. 3) enabling the application of computational techniques to study this process. In agreement with experiments, we have seen that peptides are able to enhance stalk formation in our simulations. After initiation of the vesicle fusion on sub μ s timescale, we observed lateral extension of the stalk into a curved bicelle or horseshoe-like fusion zone (Figs. 1, 2). To the best of our knowledge, such a progression of a membrane fusion zone has not been reported before, most likely because the peptides are required for its formation. Interestingly, all peptides were preferably localized at the positively curved end caps of the extending fusion zone. Besides this fusogenic activity, the peptide mixtures also ruptured GUVs, which was preceded by an apparent increase of membrane tension (Fig. S13). This tension could be caused by modifications of the bilayers surface charge density or a mass imbalance between inner and outer membrane leaflets due to peptide adsorption. Based on the membrane expansion in simulations, the outside leaflet area could increase up to 9% at full leaflet neutralization. Such an area increase is close to the maximum vesicle expansion and could lead to the enhanced bursting. However, this tension asymmetry could be reduced by peptide translocation or membrane relaxation into a highly curved membrane state, such as folds, buds, tubes, or even the previously reported sponge phase (8). Here, we show that the sponge phase forms faster than the intrinsic time resolution of our SAXS experiments (i.e., 30 s) and then coexists with the above mentioned ‘collapsed’ MLVs for up to several hours. This coexistence could be caused by local differences in concentrations of vesicles or peptides or processes with significant free energy barriers. Such processes could include peptide aggregation, refolding,

membrane translocation, fusion etc. The stochastic nature of overcoming such barriers then potentially could determine if the system locally forms MLVs or a sponge phase. Note that our findings are in agreement with observed adhesion, fusion, and rupture of membranes in LUVs near the lamellar-to-cubic phase transition, where the burst of vesicles is caused by small aggregates of sponge or cubic phase (31).

We emphasize that L18W-PGLa/MG2a interactions are obviously needed to form the sponge phase and to lead to the enhanced membrane disrupting mechanism. Such interactions, including heterodimer formation, are supported by the similar behaviour of the hybrid peptides, i.e. with L18W-PGLa and MG2a being chemically linked (2, 8, 32), although some distinct differences were observed. In particular, our video-microscopy experiments using the hybrid peptide showed bursting of the GUVs without any preceding fusion. Moreover, the vesicles burst with the hybrid peptide much faster and at lower concentration than for the equimolar L18W-PGLa:MG2a mixture (Fig. 6). Although GUVs are more susceptible to instabilities induced by AMPs, we cannot exclude that vesicle bursting also occurs in LUVs, which could be an alternative route to a sponge phase or collapsed multibilayers.

Despite the consensus among all the employed methods that peptides together are more effective and cause membrane adhesion, fusion, and further topological changes in membranes, we are aware of some limitations of all methods. The employed Martini model cannot capture a possible peptide refolding. Moreover, computer simulations are limited in a time scale to less than ms, which might not be long enough to see spontaneous membrane poration. Similarly, cryo-EM and SAXS are unlikely to have high enough spatiotemporal resolution to capture such events directly. The enhanced bursting of GUVs could be associated with increased peptide binding (and related tension increase) from the constant supply of fresh solution in the microfluidic chips. Moreover, different experiments required us to use different lipid concentrations, which could lead to different system behaviour despite the consistent [P]/[L] ratio. Such effects might be caused by the finite peptide-to-membrane partitioning, as suggested recently (9), and will be further investigated in paper IV of this series. Nevertheless, the combination of various techniques employed in this study allowed us to provide consistent molecular insight into the peptide synergism. For example, denser membrane structures, which appeared after GUVs bursting and cannot be further resolved by optical microscopy (Fig. S12), are likely to be MLVs or chunks of sponge phase based on the SAXS data.

The connection between the above findings and the biological activity of the peptides (2) is not straightforward because we do not know the molecular mechanism of membrane disruption in compositionally more complex bacteria. Therefore, it is unclear how to evaluate the fusogenic activity of peptides under in vivo conditions and if different membrane phases could play a role, e.g., in bacterial endocytosis (33).

However, the observed faster and more dramatic changes in membrane topology in our experiments correlate with the enhanced antimicrobial activity of the peptide mixture and the hybrid peptide as compared to the individual peptides.

CONCLUSION

Our real-time study of L18W-PGLa/MG2a synergism in POPE:POPG bilayers provides evidence that mutual interactions between the two peptides enhance the fusogenic and membrane disrupting properties of the individual peptides both in shortening the response time of the lipid membranes and the overall effect, such as vesicle bursting. Moreover, the rapid formation of the sponge phase suggests that the peptides, when forming heterodimers or higher order aggregates, have a pronounced ability to induce membrane curvature. Possibly this is also coupled to a preference of the peptides to a certain membrane curvature. It remains unclear, however, if these effects are correlated to an enhanced partitioning of the peptide mixture as reported recently (9). These aspects will be addressed in detail in paper IV of this series. Overall, the gain in speed and efficiency of disrupting lipid membranes seems to be key to the synergistic activity of the two peptides.

AUTHOR CONTRIBUTIONS

IK and PP carried out and analyzed all computational simulations. VG, IK, and LM performed experiments and analyzed all experimental data. KL, RD, GP, and RV designed the research. IK, VG, LM, PP, RD, GP and RV wrote the article.

ACKNOWLEDGMENTS

The authors thank Enrico Semeraro for valuable discussions. The microfluidic devices were kindly provided by the group of Tom Robinson at Max Planck institute of colloids and interfaces (Potsdam, Germany).

This work was supported by the Czech Science Foundation (grant 20-20152S), the Austrian Science Fund FWF (projects No. P 30921 and I1763-B21), and the Ministry of Education, Youths and Sports of the Czech Republic (project LL2007 under the ERC CZ program). Computational resources were provided by the CESNET LM2015042 and the CERIT Scientific Cloud LM2015085 provided under the program Projects of Large Research, Development, and Innovations Infrastructures. Additional computational resources were obtained from IT4 Innovations National Supercomputing Center – LM2015070 project supported by MEYS CR from the Large Infrastructures for Research, Experimental Development and Innovations. We acknowledge Cryo-EM core facility CEITEC MU of CIISB (CEMCOF), Instruct-CZ Centre supported by MEYS CR (LM2018127).

SUPPLEMENTARY INFORMATION

Supplementary information include movies, cryo-EM images, and input files for simulations.

REFERENCES

1. Matsuzaki, K., Y. Mitani, K. Y. Akada, O. Murase, S. Yoneyama, M. Zasloff, and K. Miyajima, 1998. Mechanism of synergism between antimicrobial peptides magainin 2 and PGLa. *Biochemistry* 37:15144–15153.
2. Leber, R., M. Pachler, I. Kabelka, I. Svoboda, D. Enkoller, R. Vácha, K. Lohner, and G. Pabst, 2018. Synergism of Antimicrobial Frog Peptides Couples to Membrane Intrinsic Curvature Strain. *Biophys J* 114:1945–1954.
3. Strandberg, E., J. Zerweck, P. Wadhvani, and A. S. Ulrich, 2013. Synergistic insertion of antimicrobial magainin-family peptides in membranes depends on the lipid spontaneous curvature. *Biophys J* 104:L9–11.
4. Aisenbrey, C., and B. Bechinger, 2014. Molecular packing of amphipathic peptides on the surface of lipid membranes. *Langmuir* 30:10374–10383.
5. Harmouche, N., and B. Bechinger, 2018. Lipid-Mediated Interactions between the Antimicrobial Peptides Magainin 2 and PGLa in Bilayers. *Biophys J* 115:1033–1044.
6. Zerweck, J., E. Strandberg, O. Kukharensky, J. Reichert, J. Bürck, P. Wadhvani, and A. S. Ulrich. Molecular mechanism of synergy between the antimicrobial peptides PGLa and magainin 2. *Sci Rep* 7:13153.
7. Pachler, M., I. Kabelka, M.-S. Appavou, K. Lohner, R. Vácha, and G. Pabst, 2019. Magainin 2 and PGLa in Bacterial Membrane Mimics I: Peptide-Peptide and Lipid-Peptide Interactions. *Biophys J* 117:1858–1869.
8. Kabelka, I., M. Pachler, S. Prévost, I. Letofsky-Papst, K. Lohner, G. Pabst, and R. Vácha, 2020. Magainin 2 and PGLa in Bacterial Membrane Mimics II: Membrane Fusion and Sponge Phase Formation. *Biophys J* 118:612–623.
9. Aisenbrey, C., M. Amaro, P. Pospíšil, M. Hof, and B. Bechinger, 2020. Highly synergistic antimicrobial activity of magainin 2 and PGLa peptides is rooted in the formation of supramolecular complexes with lipids. *Sci rep* 10:11652.
10. Abraham, M. J., T. Murtola, R. Schulz, S. Páll, J. C. Smith, B. Hess, and E. Lindahl, 2015. GROMACS: High performance molecular simulations through multi-level parallelism from laptops to supercomputers. *SoftwareX* 1-2:19–25.
11. Páll, S., M. J. Abraham, C. Kutzner, B. Hess, and E. Lindahl, 2015. Tackling Exascale Software Challenges in Molecular Dynamics Simulations with GROMACS. In E. Laure, and S. Markidis, editors, Solving software challenges for exascale, Springer, Cham, volume 8759 of *LNCS Sublibrary: SL 1 - Theoretical Computer Science and General Issues*, 3–27.
12. Marrink, S. J., H. J. Risselada, S. Yefimov, D. P. Tieleman, and A. H. de Vries, 2007. The MARTINI force field: coarse grained model for biomolecular simulations. *J Phys Chem B* 111:7812–7824.
13. Monticelli, L., S. K. Kandasamy, X. Periole, R. G. Larson, D. P. Tieleman, and S.-J. Marrink, 2008. The MARTINI Coarse-Grained Force Field: Extension to Proteins. *J Chem Theory Comput* 4:819–834.
14. de Jong, D. H., G. Singh, W. F. D. Bennett, C. Arnarez, T. A. Wassenaar, L. V. Schäfer, X. Periole, D. P. Tieleman, and S. J. Marrink, 2013. Improved Parameters for the Martini Coarse-Grained Protein Force Field. *J Chem Theory Comput* 9:687–697.
15. Bussi, G., D. Donadio, and M. Parrinello, 2007. Canonical sampling through velocity rescaling. *J Chem Phys* 126:014101.
16. Parrinello, M., and A. Rahman, 1980. Crystal Structure and Pair Potentials: A Molecular-Dynamics Study. *Phys Rev Lett* 45:1196–1199.
17. Parrinello, M., and A. Rahman, 1981. Polymorphic transitions in single crystals: A new molecular dynamics method. *J Appl Phys* 52:7182–7190.
18. Lee, J., X. Cheng, J. M. Swails, M. S. Yeom, P. K. Eastman, J. A. Lemkul, S. Wei, J. Buckner, J. C. Jeong, Y. Qi, et al., 2016. CHARMM-GUI input generator for NAMD, GROMACS, AMBER, OpenMM, and CHARMM/OpenMM simulations using the CHARMM36 additive force field. *J Chem Theory Comput* 12:405–413.
19. Bartlett, G. R., 1959. Phosphorus Assay in Column Chromatography. *J Biol Chem* 234:466–468.
20. Weinberger, A., F.-C. Tsai, G. H. Koenderink, T. F. Schmidt, R. Itri, W. Meier, T. Schmatko, A. Schröder, and C. Marques, 2013. Gel-Assisted Formation of Giant Unilamellar Vesicles. *Biophys J* 105:154–164.
21. Amenitsch, H., M. Rappolt, M. Kriechbaum, H. Mio, P. Laggner, and S. Bernstorff, 1998. First performance assessment of the small-angle X-ray scattering beamline at ELETTRA. *J Synchrotron Radiat* 5:506–508.
22. Hammersley, A. P., S. O. Svensson, M. Hanfland, A. N. Fitch, and D. Hausermann, 1996. Two-dimensional detector software: From real detector to idealised image or two-theta scan. *High Press* 14:235–248.

23. Marx, L., E. F. Semeraro, J. Mandl, J. Kremser, M. P. Frewein, N. Malanovic, K. Lohner, and G. Pabst, 2021. Bridging the Antimicrobial Activity of Two Lactoferricin Derivatives in *E. coli* and Lipid-Only Membranes. Front Med Technol 3:625975.
24. Yandrapalli, N., and T. Robinson, 2019. Ultra-high capacity microfluidic trapping of giant vesicles for high-throughput membrane studies. Lab Chip 19:626–633.
25. Pozo Navas, B., K. Lohner, G. Deutsch, E. Sevcsik, K. A. Riske, R. Dimova, P. Garidel, and G. Pabst, 2005. Composition dependence of vesicle morphology and mixing properties in a bacterial model membrane system. Biochim Biophys Acta 1716:40–48.
26. Dimova, R., S. Aranda, N. Bezlyepkina, V. Nikolov, K. A. Riske, and R. Lipowsky, 2006. A practical guide to giant vesicles. Probing the membrane nanoregime via optical microscopy. J Phys Condens Matter 18:S1151–S1176.
27. Walde, P., K. Cosentino, H. Engel, and P. Stano, 2010. Giant Vesicles: Preparations and Applications. Chem Bio Chem 11:848–865.
28. Dimova, R., and C. Marques, 2019. The Giant Vesicle Book. Taylor & Francis Group, LLC, Boca Raton.
29. Dimova, R., 2019. Giant Vesicles and Their Use in Assays for Assessing Membrane Phase State, Curvature, Mechanics, and Electrical Properties. Ann Rev Biophys 48:93–119.
30. Fenz, S. F., and K. Sengupta, 2012. Giant vesicles as cell models. Integr Biol 4:982–995.
31. Ellens, H., D. P. Siegel, D. Alford, P. L. Yeagle, L. Boni, L. J. Lis, P. J. Quinn, and J. Bentz, 1989. Membrane fusion and inverted phases. Biochemistry 28:3692–3703. PMID: 2751990.
32. Nishida, M., Y. Imura, M. Yamamoto, S. Kobayashi, Y. Yano, and K. Matsuzaki, 2007. Interaction of a magainin-PGLa hybrid peptide with membranes: insight into the mechanism of synergism. Biochemistry 46:14284–14290.
33. Lonhienne, T. G. A., E. Sagulenko, R. I. Webb, K.-C. Lee, J. Franke, D. P. Devos, A. Nouwens, B. J. Carroll, and J. A. Fuerst, 2010. Endocytosis-like protein uptake in the bacterium *Gemmata obscuriglobus*. Proc Natl Acad Sci USA 107:12883–12888.

Figure 1

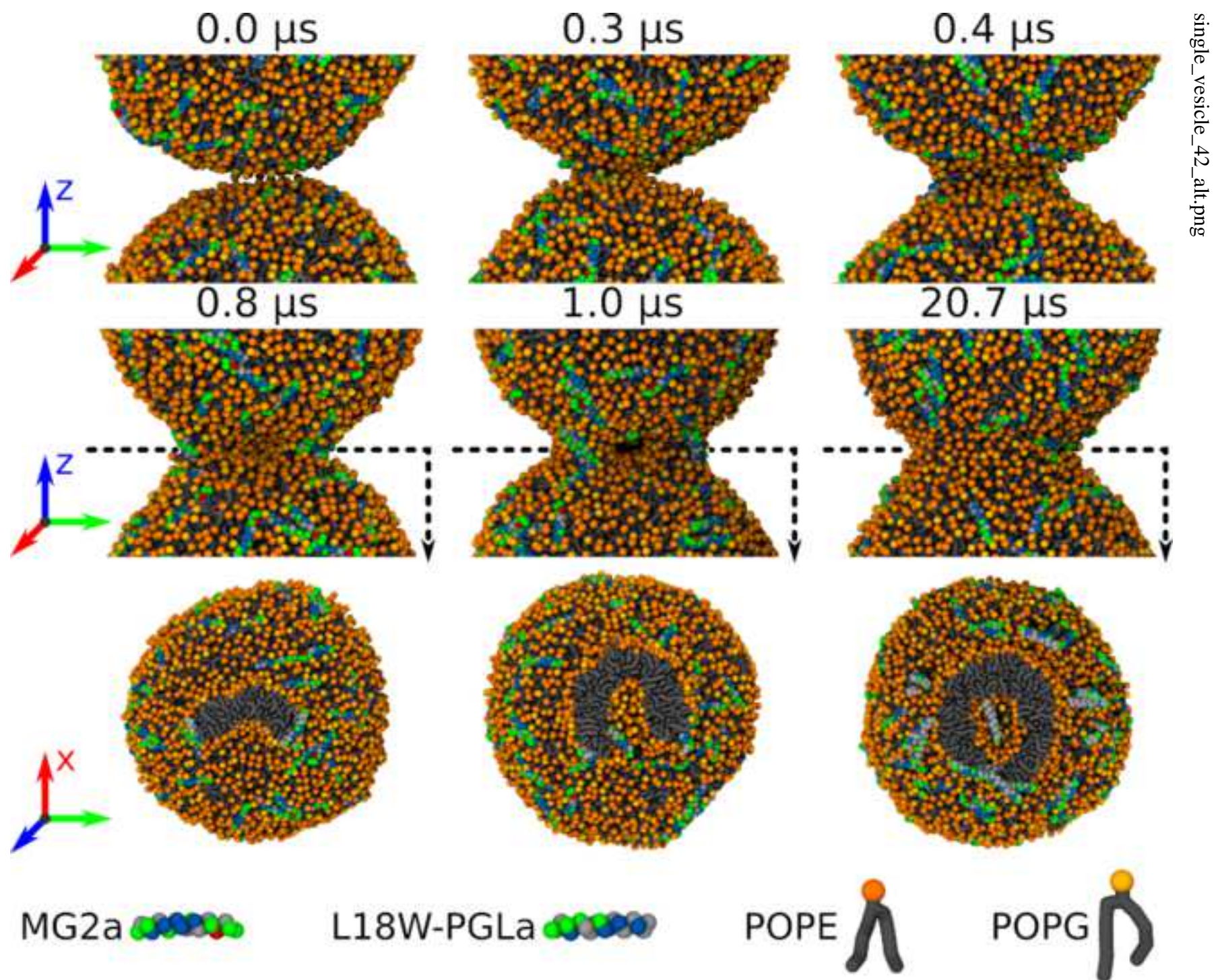
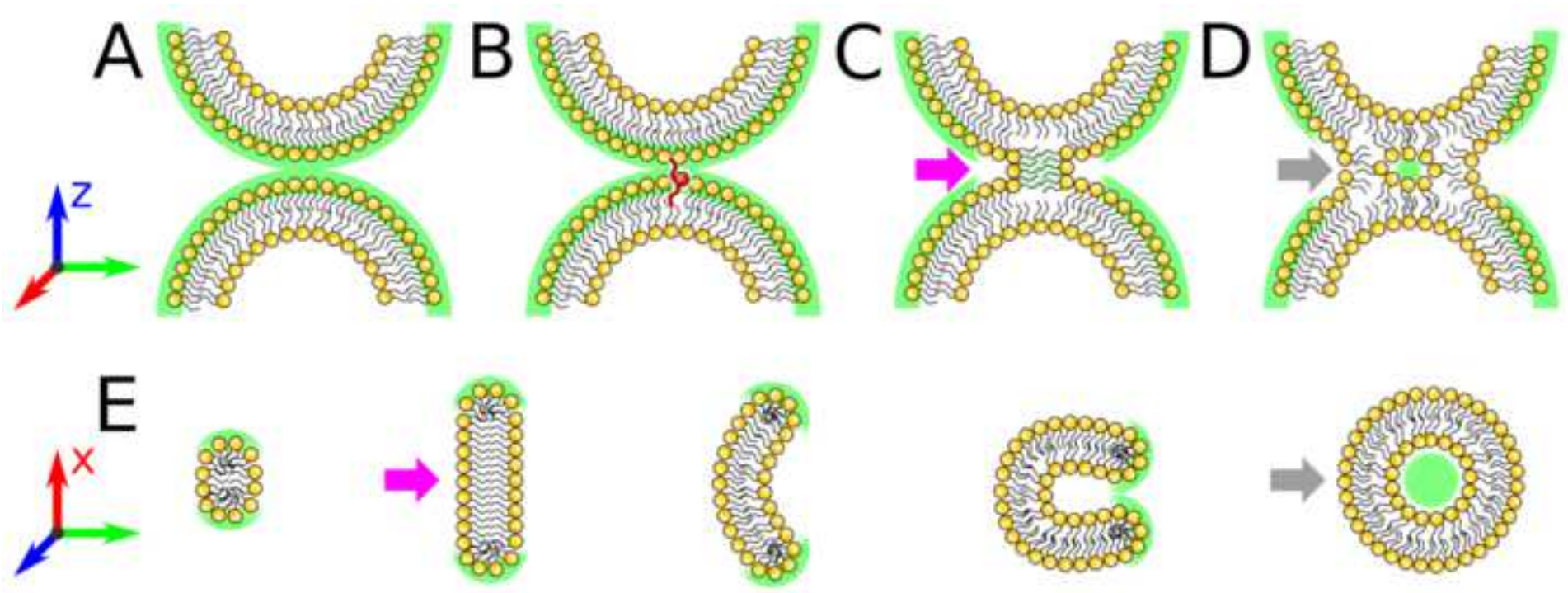


Figure 2

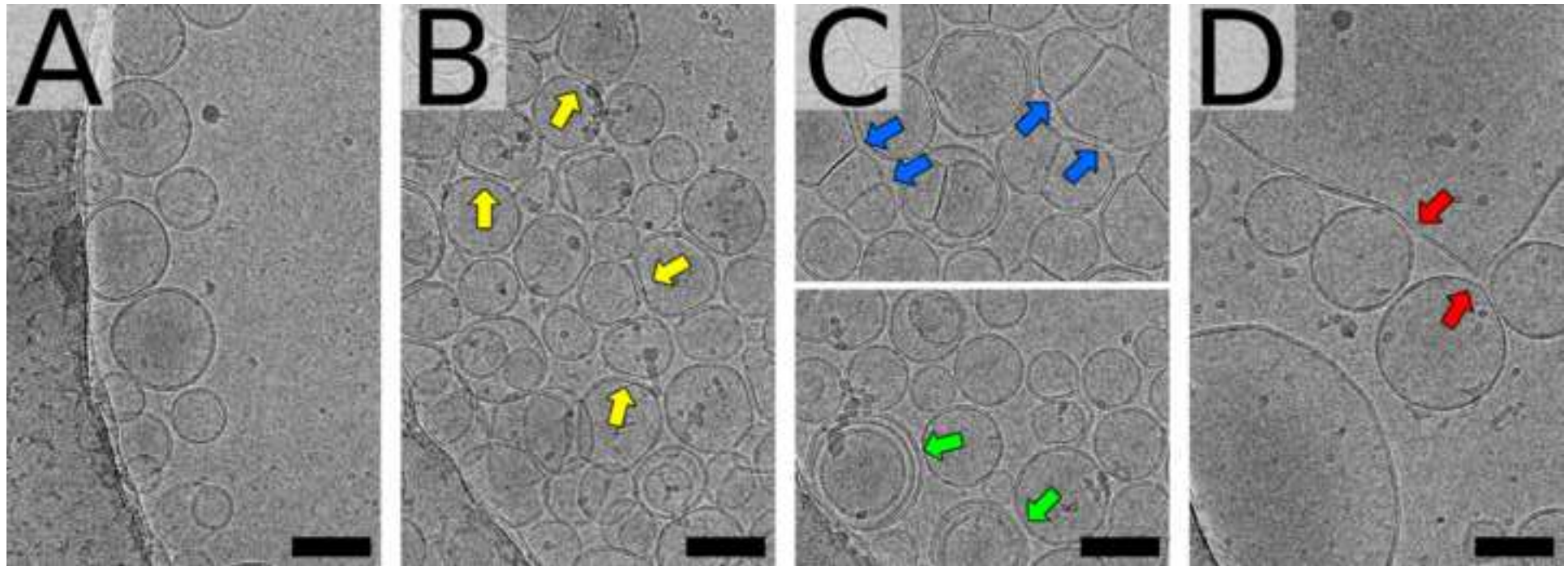
[Click here to access/download;Figure;figure2.tif](#)



single_vesicle_42_sketchy.png

Figure 3

[Click here to access/download;Figure;figure3.tif](#)



cen_ml.png

Figure 4

[Click here to access/download;Figure;figure4.tif](#)

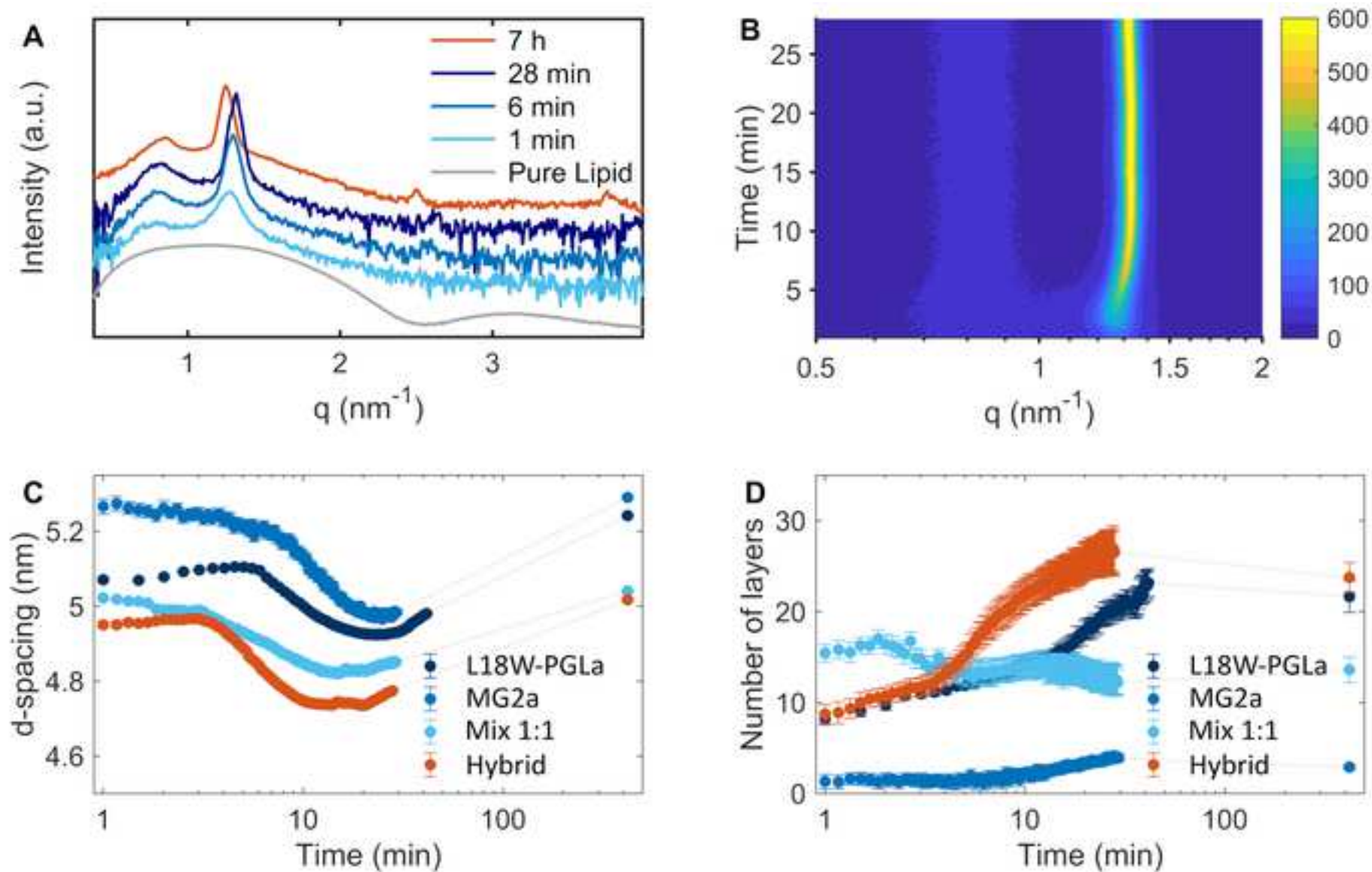
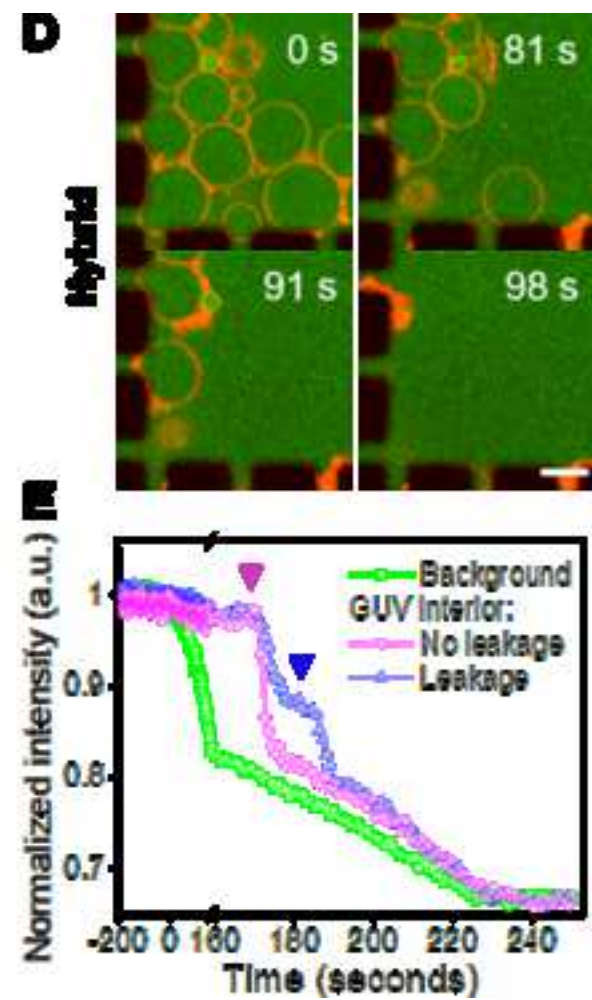
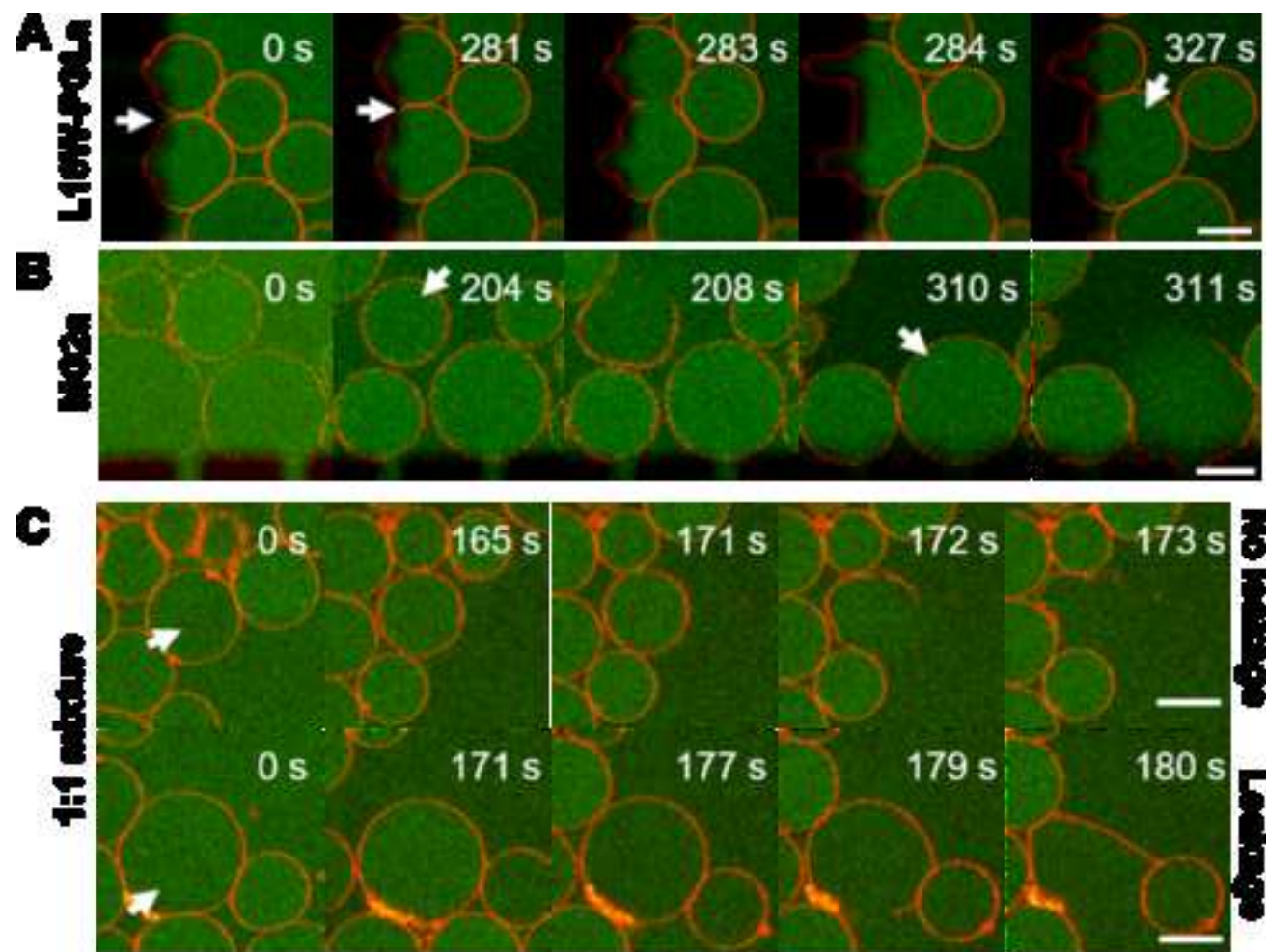


Figure 5

[Click here to access/download;Figure;figure5.tif](#)



Figure_5.png

Figure_6.png

